A global picture of laser-driven radiobiology and the PoPLaR experiment

J. McGarrigle [1], C. Dyson [1], E.Doiler [3], E.Melia [4], E. Tassano-Smith [1], K. Long [1,2]

1. *Imperial College London, Exhibition Road, London, SW7 2AZ, UK*
2. *STFC Rutherford Appleton Laboratory, Harwell Oxford, Didcot, OX11*
3. *University of Strathclyde, Glasgow, G4 0NG*
4. *University of Birmingham, Edgbaston,Birmingham B15 2TT, UK*

Abstract

Laser-driven proton and ion sources deliver nanosecond-scale bunches at instantaneous dose rates of 10^7–10^9 Gy/s, but their broad spectra, large divergence and shot-to-shot variability mean that the field delivered to a biological sample is defined by the complete source-to-sample system. This technical note has two purposes: to establish the current global standing of laser-driven radiobiology and to use this to assess the Proof-of-Principle LhARA Radiobiology experiment (PoPLaR) at SCAPA against the current field. This will determine areas of prioritisation in the field and guide the next phase of the PoPLaR design.

A systematic review study identified 22 publications (2009–2025) on laser-driven proton and ion radiobiology, including *in vitro* and *in vivo* experiments across both normal and tumour cell studies. Irradiation conditions were compiled and analysed to search for trends in the global body of published work. The data exhibited an overall increase in maximum particle energy by publication year ($r = 0.921$, $p = 4.97 \times 10^{-10}$), showing progression in the field over time.

The global dataset is dominated by both proton and *in vitro* studies, with only four *in vivo* experiments and only a single non-proton ion study (carbon). A minimum reporting standard for the field is recommended in order to directly compare studies as there appears to be inconsistent reporting of beam characteristics.

Examining the global biological data, a difference is observed between tissue types in the laser-driven dataset: normal tissue cells appear to exhibit steeper survival curves than tumour cells under laser-driven proton irradiation. Conventional proton data, by contrast, show both normal and tumour cell survival curves exhibit comparable steepness to that of the laser-driven normal tissue curves. No other trends can be deciphered between survival and beamline parameters, or in the global γH2AX foci detection data, due to limited available data.

PoPLaR successfully transported protons from the SCAPA source ($\sim$6 J, $\sim$25 fs pulses on 12.7 μm Kapton; median fitted cutoff 11.8 MeV over 48 Thomson-parabola shots) through a 150 T m^{-1} PMQ doublet and Cu scatterer to a 2.7 cm^2 cell-dish field. FaDu cells received 0.57 ± 0.03 Gy per shot with a spatial coefficient of variation of 13.9%, during the first biological phase of PoPLaR. The irradiation energy, dose and field size recorded during the PoPLaR experiments align with the other reported *in vitro* experiments in the field. The preliminary survival data is within the order of the global data but trends are not distiguishable at this stage. Limitations with PoPLaR is dominated by dose control: the dose fluctuation of 24–38% per multi-shot exposure and the absence of an on-shot diagnostic. These properties should be prioritised for the next phase of PoPLaR experiments.

1 Introduction

Conventional proton and ion accelerator facilities typically include a particle source, injector and accelerator. These technologies provide highly controllable beams with well-defined energy and dosimetry but they often require substantial infrastructure, particularly when ion energies must be to the tens or hundreds of MeV for biomedical applications.

Laser-driven ion acceleration offers an alternative, using an intense laser pulse focused onto a solid or gas target, producing a plasma system (TNSA) that accelerates protons and heavier ions in bunches from the rear surface. These bunches contain lots of particles and can irradiate samples within nanoseconds at instantaneous dose rates of 10^7 to above 10^9 Gy s^{-1} [1–4]; single pulses delivering close to 20 Gy in under 10 ns have recently been reported [4]. This is advantageous for more modern radiotherapy techniques like FLASH, which uses ultra-high dose rate beams to spare normal tissue.

LhARA is conceived as a laser-hybrid accelerator dedicated to the study of understanding the biological response to proton and ion beams, with particular emphasis on control of energy, temporal structure, spatial structure and dose rate beyond what is routinely available at conventional clinical facilities. To improve on the current phase of LhARA's development, an analysis of the current laser-driven radiobiology field has been carried out and documented in this technical note.

The purpose of this technical note is to examine what has been established experimentally about the laser-driven beams capable of delivering radiobiological experimentation, and the corresponding biological response to laser-driven proton and ion beams. This allows for global patterns to be established, to assess what stage of development LhARA is currently in in comparison and to determine the capabilities required at LhARA in the future.

2 Materials and Methods

The primary focus of this study was the identification of global trends across radiobiological experiments performed with laser-driven proton or ion beams. This study include 22 publications on laser-driven proton and ion radiobiology published between 2009 and 2025; 21 of which investigate protons only [1–21]; and 1 carbon-ion study [22]. The publications varied in type of radiobiological study. Of the experiments detailed across all 22 publications, 4 were carried out *in vivo*, made up of 3 zebrafish embryo studies [4, 8, 20] and 1 mouse ear study [5]. The remaining studies were carried out *in vitro*, encompassing 46% normal and 54% tumour cell studies, giving a balanced overview of the *in vitro* field.

3 Search Criteria

The literature search was designed to collect the maximum amount of publications including a laser-driven proton or ion beam incident on a biological sample. Relevant publication search engines were searched using the terms *laser* and *radiobiology* and for each relevant publication, the citations were also investigated for further papers.

Each publication was assessed using pre-determined eligibility criterion. The eligibility PICO framework (population, intervention, comparison and outcome) used to guide inclusion is summarised in Table 1. The population comprised *in vitro* or *in vivo* biological models. The intervention was determined to be irradiation with a laser-driven proton or ion beam. A comparison was not mandatory, but where present included an unirradiated control, conventional proton irradiation, photon or X-ray irradiation, different oxygenation conditions, or an alternative temporal dose-delivery scheme. The required outcome was that the feasibility was demonstrated. The PICO framework used to guide inclusion is summarised in table 1.

Table 1: Population, Intervention, Comparison and Outcome (PICO) framework used to screen studies for inclusion in the present review.

Population	**Intervention**
In vitro cells, three-dimensional spheroids, zebrafish embryos, or small-animal *in vivo* models	Irradiation with a laser-driven proton or ion beam
Comparison	**Outcome**
X-ray or CAP reference	Feasibility of setup demonstrated

Publications were excluded when they described only laser acceleration, beamline development, focusing, dosimetry or facility design without a biological sample, when they were reviews rather than primary experimental reports, or when the biological experiment used only a conventionally accelerated beam.

The combined search routes identified 32 candidate publications for screening. The literature-selection process is summarised in the PRISMA-flow diagram provided in figure 1.

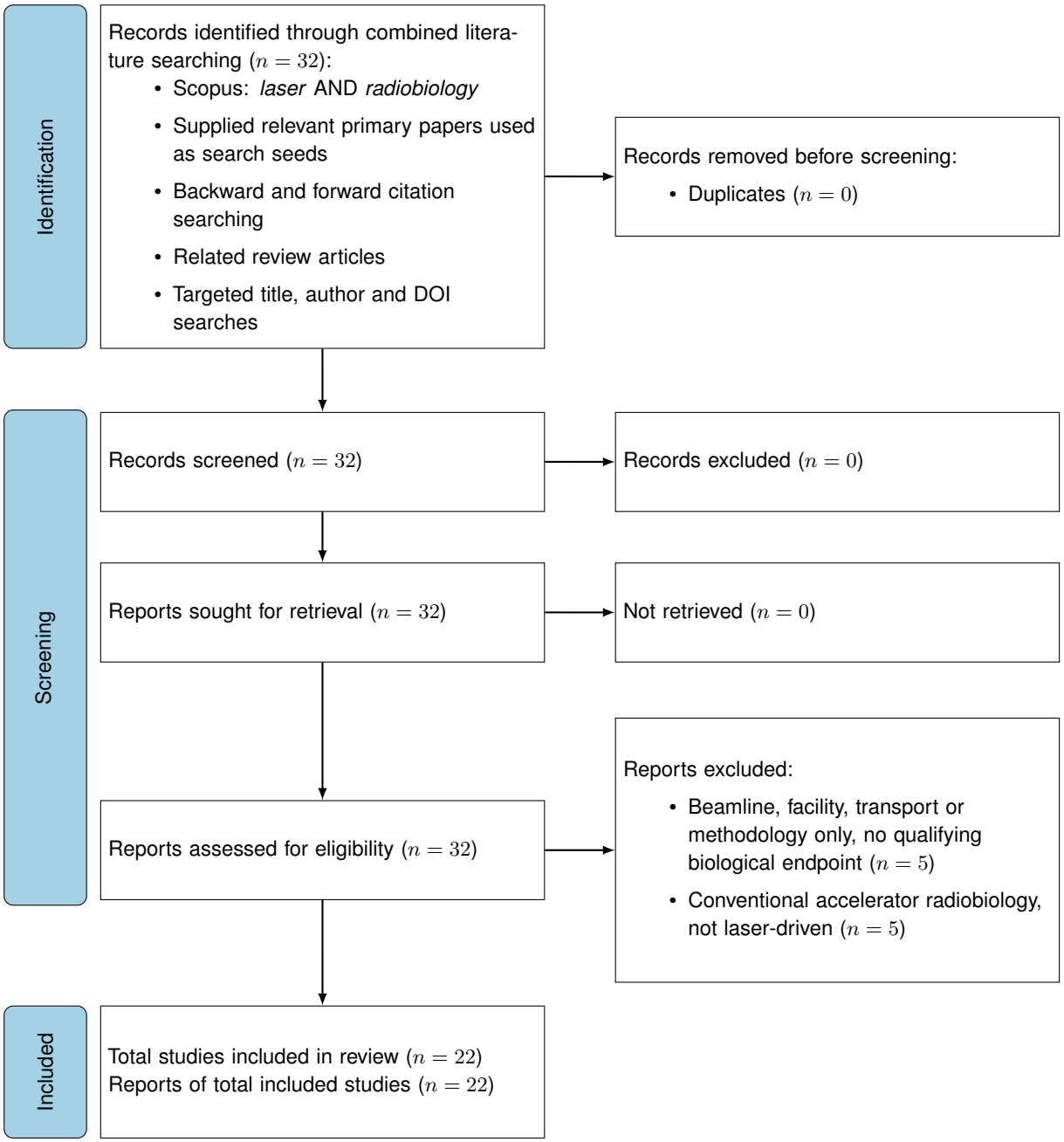


Figure 1: PRISMA flow diagram summarising identification, screening, eligibility assessment and inclusion of studies for the present review.

As illustrated in figure 1, no duplicate publications were identified, and all 32 reports were available for full-text assessment. Ten publications were excluded after eligibility review: five were beamline, facility, transport or methodology studies without a radiobiological endpoint, and five were radiobiology studies performed with conventional accelerator beams rather than laser-driven particles. A total of 22 publications therefore satisfied the inclusion criteria and were retained for data extraction, listed in table 2 with titles, paper ID and references.

Table 2: Details of all included publications, including title, IDs and bibliography references

Paper ID	Paper title	Reference
1	Laser driven FLASH radiobiology using a high dose and ultra high dose rate single pulse proton source	[4]
2	Cellular irradiations with laser-driven carbon ions at ultra-high dose rates	[22]
3	A new platform for ultra-high dose rate radiobiological research using the BELLA PW laser proton beamline	[3]
4	Tumour irradiation in mice with a laser-accelerated proton beam	[5]
5	Ultra-High Dose Rate FLASH Irradiation Induced Radio-Resistance of Normal Fibroblast Cells Can Be Enhanced by Hypoxia and Mitochondrial Dysfunction Resulting From Loss of Cytochrome C	[6]
6	Spectral and spatial shaping of laser-driven proton beams using a pulsed high-field magnet beamline	[7]
7	A feasibility study of zebrafish embryo irradiation with laser-accelerated protons	[8]
8	Fast dose fractionation using ultra-short laser accelerated proton pulses can increase cancer cell mortality, which relies on functional PARP1 protein	[9]
9	DNA DSB Repair Dynamics following Irradiation with Laser-Driven Protons at Ultra-High Dose Rates	[2]
10	The radiobiology of laser-driven particle beams: focus on sub-lethal responses of normal human cells	[10]
11	Ultra-short laser-accelerated proton pulses have similar DNA-damaging effectiveness but produce less immediate nitroxidative stress than conventional proton beams	[11]
12	Dose-controlled irradiation of cancer cells with laser-accelerated proton pulses	[12]
13	A laser-driven nanosecond proton source for radiobiological studies	[13]
14	Biological effectiveness on live cells of laser driven protons at dose rates exceeding 10^9 Gy/s	[1]
15	Dosimetry and spectral analysis of a radiobiological experiment using laser-driven proton beams	[14]
16	Measurement of relative biological effectiveness of protons in human cancer cells using a laser-driven quasimonoenergetic proton beamline	[15]
17	Dose-dependent biological damage of tumour cells by laser-accelerated proton beams	[16]
18	Application of laser-accelerated protons to the demonstration of DNA double-strand breaks in human cancer cells	[17]
19	Measurement of DNA Double-Strand Break Yield in Human Cancer Cells by High-Current, Short-Duration Bunches of Laser-Accelerated Protons	[18]
20	Development of a portable hypoxia chamber for ultra-high dose rate laser-driven proton radiobiology applications	[19]
21	The dresden platform is a research hub for ultra-high dose rate radiobiology	[20]
22	ELIMAIA-ELIMED: a new user platform for radiobiological research utilizing laser-driven protons	[21]

3.1 Beam/sample correlation analysis

To analyse the relationships between the beam and sample parameter values, a Pearson correlation coefficient analysis was carried out. For two parameter variables x and y, the Pearson coefficient was calculated as

$$r = \frac{\sum_i (x_i - \bar{x})(y_i - \bar{y})}{\sqrt{\sum_i (x_i - \bar{x})^2}\sqrt{\sum_i (y_i - \bar{y})^2}}, \tag{1}$$

where n is the number of measurements in the sample, the x_i are the values of the beam parameters, the y_i are the associated quantitative outcomes, and the mean of the x_i and y_i are $\bar{x}$ and $\bar{y}$, respectively. For this study, $|r| > 0.5$ is classified as a 'strong correlation', r in the range $0.3 < |r| \leq 0.5$ is classified as a moderate correlation, and $|r| \leq 0.3$ is classified as a weak correlation. [23]

The statistical significance of each Pearson correlation coefficient was evaluated to determine which beam/sample parameters exhibited the strongest evidence of correlation. This was assessed by testing the null hypothesis of zero correlation ($r = 0$) using the test statistic t, defined in equation 2.

$$t = r\sqrt{\frac{n-2}{1-r^2}}\,; \tag{2}$$

where r is the Pearson correlation coefficient and n is the sample size. [24]

Under the null hypothesis, t follows Student's t-distribution with $n-2$ degrees of freedom. A two-tailed p-value was calculated as the probability of observing a test statistic at least as extreme as the measured value, assuming that the null hypothesis is true [24]. Correlations with $p < 0.05$ were considered statistically significant, with smaller p-values indicating stronger evidence against the null hypothesis.

Where useful to visually examine the trends observed in the data, scatter plots were generated. Since the expected distribution of the data is unknown, a simple straight-line fit was applied to each graph to broadly visualise whether correlations are increasing, decreasing, or absent, rather than to assume any underlying linearity or normal distribution. The straight-line fit was used to determine the 95% confidence interval, CI, and the 95% prediction interval, PI, calculated using Equations 3 and 4, respectively.

$$\mathrm{CI} = \hat{y} \pm t_{\mathrm{crit}} \cdot \sigma \sqrt{\frac{1}{n} + \frac{(x-\bar{x})^2}{(\hat{x}-\bar{x})^2}}; \tag{3}$$

$$\mathrm{PI} = \hat{y} \pm t_{\mathrm{crit}} \cdot \sigma \sqrt{1 + \frac{1}{n} + \frac{(x-\bar{x})^2}{(\hat{x}-\bar{x})^2}}; \tag{4}$$

where $\hat{y}$ is the end point values, t_{crit} is the statistic of interval confidence, also known as the critical value of the t distribution ([25]), σ is the squared deviation of the end point values, x is an array of evenly spaced x values for the range of each beam parameter, $\bar{x}$ is the mean of the beam parameters. [25]

3.2 Biological data analysis

3.2.1 Survival data

Among the 22 publications retained in the dataset, 7 published survival curves displaying the normalised survival vs dose for their *in vitro* laser-driven proton experiments. Where raw data was unable to be located, published survival and DNA-damage figures were digitised with using MATLAB software to calibrate the axes of each plot and manually select points and error bars, in order to convert to define co-ordinate on the graph.

The zero-survival observations reported are plotted on a visual floor when a logarithmic axis is required, but are excluded from logarithmic linear regression (as $\log(0)$ is not defined). Conventional-proton reference curves were extracted from HUVEC data in Paper 10 and SKX data in Paper 12, included to compare the laser-driven data to both normal and tumour cells.

To investigate whether beam parameters influence the steepness of the survival curves, several survival metrics were calculated for each curve. First, a log-linear fit was used to estimate the rate at which cell survival decreases with dose:

$$\log_{10} S(D) = a + mD, \tag{5}$$

where S is the normalised surviving fraction, D is dose, and m is the fitted slope in Gy^{-1}. A more negative m indicates a steeper decrease in survival with increasing dose. This provides a simple measure of the overall curve steepness. [26]

Second, each survival curve was fitted with the linear-quadratic (LQ) model,

$$S(D) = \exp\left[-\alpha D - \beta D^2\right], \tag{6}$$

where S is the surviving fraction after dose D. The parameter α (Gy^{-1}) describes cell killing that is proportional to dose, and β (Gy^{-2}) describes the additional killing that grows with dose squared.[26]

Each fit was then summarised by extracting α, β, the local slope at 2 Gy and D_{10} metrics so that curves could be compared with beam parameters. D_{10} is the dose that leaves 10% of cells surviving. Setting $S = 0.1$ in equation (6) gives $\alpha D + \beta D^2 = \ln 10$.

$$D_{10} = \frac{2\ln 10}{\alpha + \sqrt{\alpha^2 + 4\beta \ln 10}}, \tag{7}$$

written in this form because it stays numerically stable when β is very small.[26] A lower D_{10} means the cells are more radiosensitive.

The correlations between the extracted survival metrics and the beam parameters were analysed using the same method detailed in section 3.1 to explore links between survival and beam setup.

3.2.2 γH2AX data

Of the 22 publications, there were 5 that published plots of γH2AX foci changes with dose. This was reduced to 4 publications (5 experiments) to keep time of fixation consistent. The data was therefore limited to experiments whereby the fixing for γH2AX foci detection occured between 30 minutes to 1 hour after laser-driven proton irradiation. This included data from Paper 13 (using HeLa cells) and Paper 19 (A549 cells) collected around 30 minutes post-irradiation and Paper 8 (SF763 and U87-MG cells) and Paper 11 (A549 cells) collected around the 1 hour time point. Similar to the survival data, plots were digitised where values were not provided.

3.3 Limitations of the approach

The dataset is small (22 publications) and dominated by a limited amount of facilities, so repeated use of one beamline produces repeated parameter values that can inflate correlations. Parameters are often also sparsely/ inconsistently reported. Additionally, only one included study used carbon ions and only four experiments used *in vivo* models, none deeper than the mouse ear.

4 The field of laser-driven radiobiology

Mapping out the number of publications by year shows a fall off in publications in recent years, evident by figure 2. The 22-paper set contains 2 papers in 2009–2010, 5 in 2011–2012, one each in 2013–2014, 2015–2016 and 2017–2018, 4 in 2019–2020, 4 in 2021–2022, 2 in 2023–2024 and 2 in 2025–2026. Both publications in the 2025–2026 column were published in 2025, with currently 0 publications this year, at the time of this technical note. This is likely due to the increase in complexity required to publish increasing to be notable or 'novel' in the field, earlier publications being possible with only a proof-of-principle experiment.

The publications seem to be dominated by Scientific Reports, yielding 32% of the publications, as illustrated in figure 3, likely due to the interdisciplinary nature and scope of this research field, which makes it a suitable journal for such articles over niche journals.

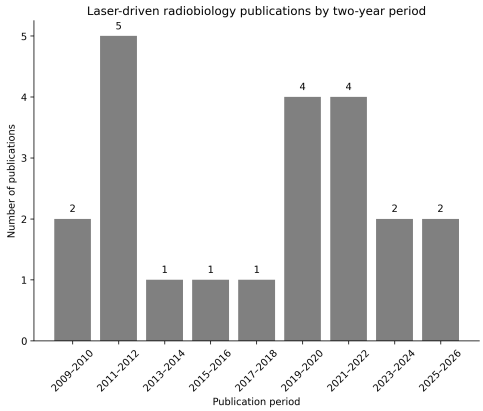


Figure 2: Publication frequency over time in two-year periods.

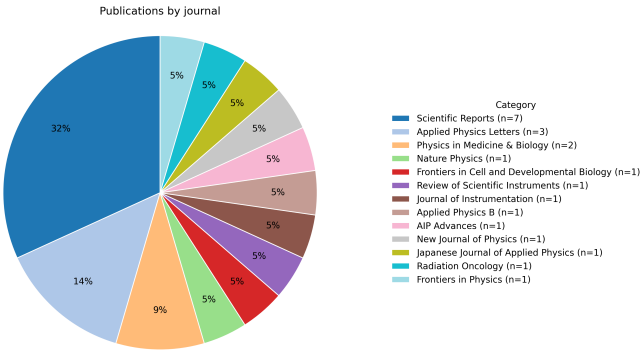


Figure 3: Publication amounts by journal.

Figure 4 details the geographical location of each publication. Publications emerging from Germany contribute 8 of the 22 publications, the United Kingdom 5, France and Japan 3 each, with single publications from the United States, China and Czechia.

Figure 5 divides the publications by beamline used, identifying DRACO as the most used beamline for laser-driven radiobiological experiments, followed by J-KAREN, LULI PICO2000 and TARANIS.

Radiochromic film (RCF) is the most frequently used primary method for determining dose at the sample, being used in 55% of the publications either in isolation (paired with image processing software) or in conjunction with other dosimetry systems, see figure 6. This is likely due to its compact nature, insensitivity to electromagnetic pulse pickup and ability to provide two-dimensional spatial information. RCF is limited in terms of time, taking up to 24 hours to get full dosimetry information, making it difficult to use with clonogenics due to the seeding densities post plating relying on knowing the dose delivery.

Unlike the dosimetry systems, the target material of the laser source was not dominated by any particular material: gold, plastic, titanium and aluminium are the most common target materials in the global data, making up 14% each of the number of publications (figure 7). This also likely overlaps with repetition in beamline use and the sharing of sources.

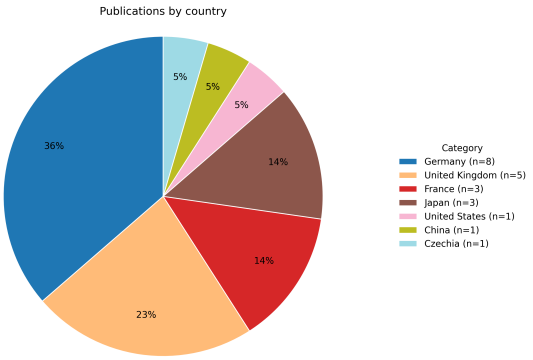


Figure 4: Publication amounts by country.

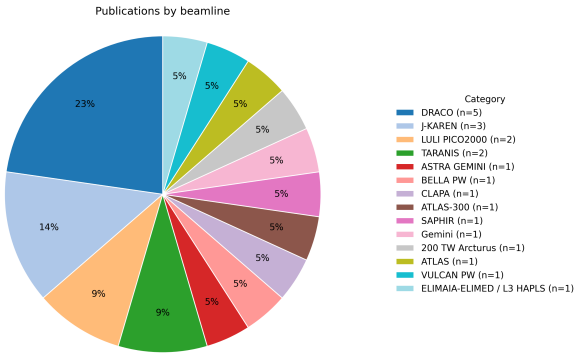


Figure 5: Publication amounts by beamline/facility.

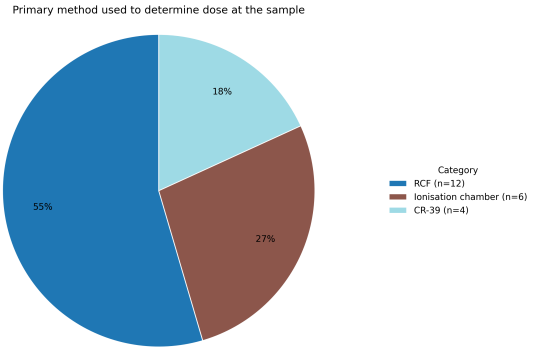


Figure 6: Sample dosimetry system used.

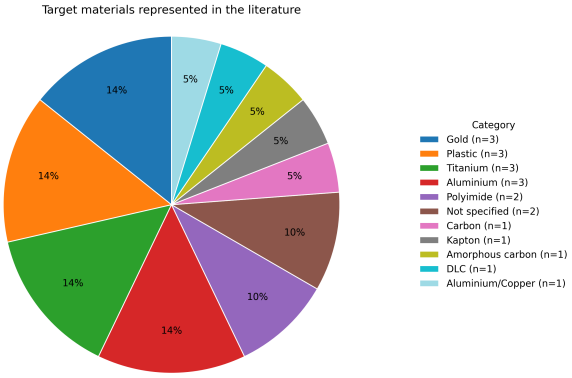


Figure 7: Target materials used.

5 The laser-driven radiobiology parameter space

Figure 8 summarises the Pearson correlations across the source and sample parameter values reported in the 22 publications.

Examining trends by year to look at the evolution of laser-driven beams, there is a notable statistically significant positive correlation in reported maximum particle energy with year: $r = 0.921$, $p = 4.97 \times 10^{-10}$, $n = 23$, see figure 9. This is compelling evidence of increased capabilities of laser-driven beams over time, being able to deliver increasingly more energy at the sample location. Continued progress in the field along this trajectory allows to move toward conventionally accelerated proton energies and allows for larger animal models and deeper seated tumour irradiations *in vivo*.

When considering if any of the source parameters correlate, the strongest correlation appears to be between Peak Intensity and Cutoff Energy ($r = 0.995$, $p = 1.51 \times 10^{-12}$, $n = 13$)), closely followed by Particle Energy Max and Cutoff Energy ($r = 0.995$, $p = 2.76 \times 10^{-11}$, $n = 12$).

While the positive correlation between peak intensity and proton cutoff energy is realistic, since higher laser intensities can generate hotter and more numerous fast electrons and therefore a stronger rear-surface sheath field in TNSA, allowing protons to reach higher maximum energies, figure 10 suggests that the strength of this relationship may also be influenced by repeated observations, in particular at the high intensity end, likely due to repeated use of a small number of high-performance beamlines.

The same interpretation applies to the strong positive correlation between maximum particle energy and cutoff energy shown in figure 11: the relationship is physically expected, since both quantities reflect the high-energy extent of the accelerated proton spectrum, but the apparent strength of the correlation may also be enhanced by clustering of repeated measurements at the extremes, arising from repeated use of a small number of high-performance beamlines.

Comparing the laser-driven source parameters to the sample parameters, the strongest observed correlation is the negative relationship between cutoff energy and reported relative dose variation ($r = -0.771$, $p = 1.13 \times 10^{-4}$, $n = 19$). This could be due to higher-energy protons being transported more efficiently and being less sensitive to energy loss through the beamline. However, cutoff energy also anticorrelates with reported dose ($r = -0.722$, $p = 2.20 \times 10^{-4}$, $n = 21$), suggesting that increasing cutoff energy may come with a reduction in delivered fluence and therefore dose. Additionally, figure 12 suggests that the data points at the 40 MeV cutoff-energy extremity may be disproportionately influencing the correlation and dominating the fit.

Maximum particle energy correlates with irradiated area ($r = 0.786$, $p = 1.86 \times 10^{-4}$, $n = 17$), representing the second strongest correlation between source and sample parameters. figure 13 illustrates this positive relationship. This is likely because

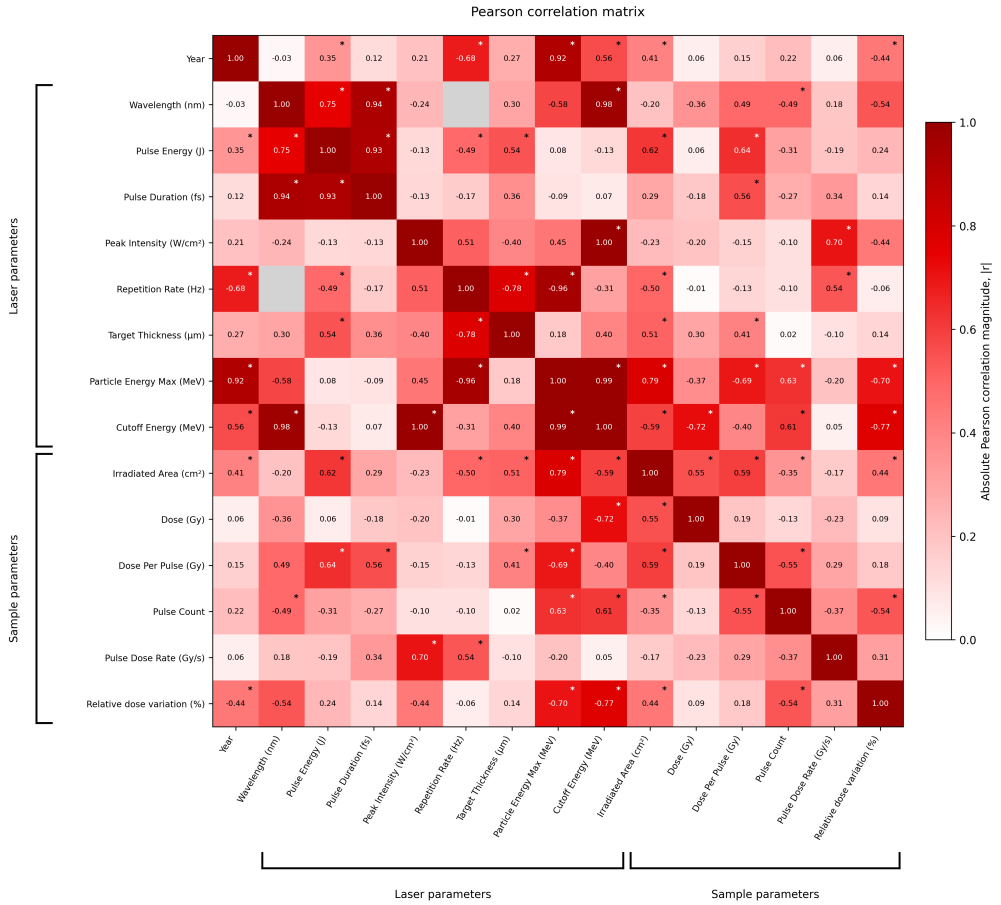


Figure 8: Pearson correlation matrix for the source and sample parameter values reported in the 22 publications. White corresponds to $r = 0$ and deeper red to larger $|r|$; annotated with the r value. Asterisks mark statistically significant correlations (indicated by $p < 0.05$). Grey/unannotated cells correspond to there not being enough data to calculate a correlation.

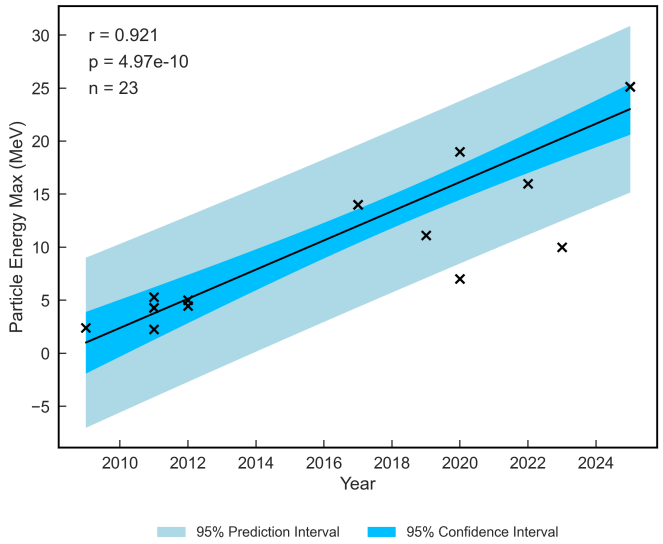


Figure 9: Plot to show how the maximum particle energy during experiments changes depending on the year of the publication.

higher-energy proton beams can be transported and shaped over larger fields more effectively, allowing the transport system to sacrifice more phase space through collimation and scattering while still retaining sufficient transmission for biologically useful irradiation.

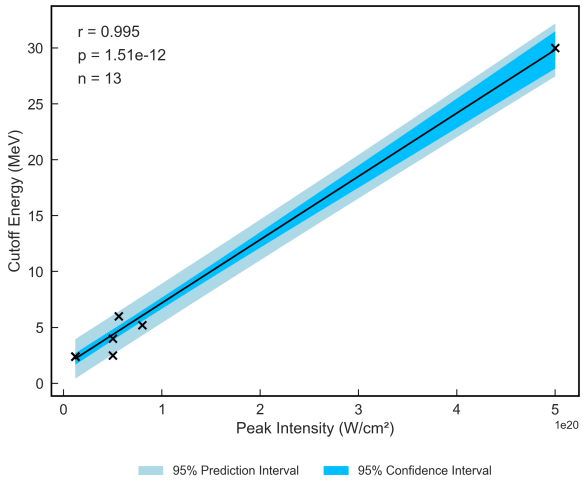


Figure 10: Plot of Peak Intensity vs Cutoff Energy.

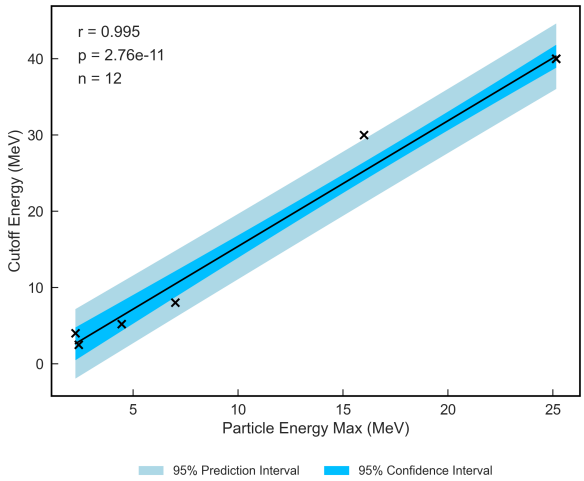


Figure 11: Plot of Particle Energy Max vs Cutoff Energy.

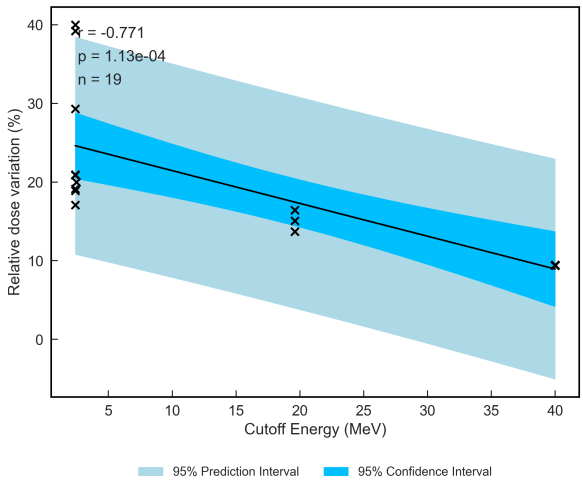


Figure 12: Plot of Dose Variation vs Cutoff Energy.

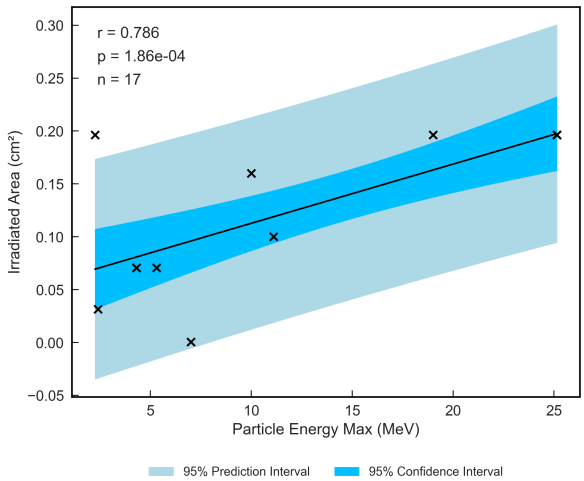


Figure 13: Plot of Particle Energy Max vs Irradiation Area.

6 Global *in vitro* laser-driven radiobiological results

6.1 Clonogenic Survival

The extracted survival data is displayed in figure 14, illustrating the range of cell lines and dose-response shapes. The data shows no distinct pattern, likely due to the varying cell line and beam parameters. Notably, there are 2 experiments that used U87-MG cell lines, indicated by the blue markers. These markers seem to overlap, with error bars accounting for differences in the data, regardless of their respective experiments being carried out at different beamlines. This suggests that beam parameters affect the survival less than cell line choice. This is validated by figure 15, demonstrating that colouring the markers by beamline shows no overlap in data when the same facility is used.

Figure 16 demonstrates that colouring the markers by tissue type (normal or tumour) appears to result in more a distinctive trend. Normal-cell datasets such as HUVEC and V79 appear much steeper, while some tumour lines are comparatively resistant; Paper 3 is unusual in reporting a large normal-versus-tumour separation under its specific conditions.

To check if this is purely the result of cell line radiosensitivities, 2 references were added– 1 tumour (SKX, Paper 12) and one normal tissue (HUVEC, Paper 10) cell line that were irradiated by conventionally accelerated protons. Both of the reference survival curves follow the normal tissue pattern, despite SKX being a tumour cell line, see figure 17.

As detailed in section 3.2.1, survival metrics were extracted from a linear quadratic fit of each survival curve to see how beam parameters may influence the survival of the cells. This is displayed in figure 18.

There are no statistically significant correlations between the beam parameters and survival metrics when evaluating all cell lines together. This further suggests that beam parameters are less influential on the survival than cell line selection.

When separating the cell lines into normal and tumour cells, there appears to be 3 statistically significant correlations, all with Peak Intensity. These are: α (normal cells), α (tumour cells) and slope at 2 Gy (tumour cells). Plotting these correlations as a scatter plot shows that these correlations are largely driven by a single point at the Peak Intensity extremity (see Figures 19, 20 and 21). The database must have more data to be able to evaluate the survival curves effectively.

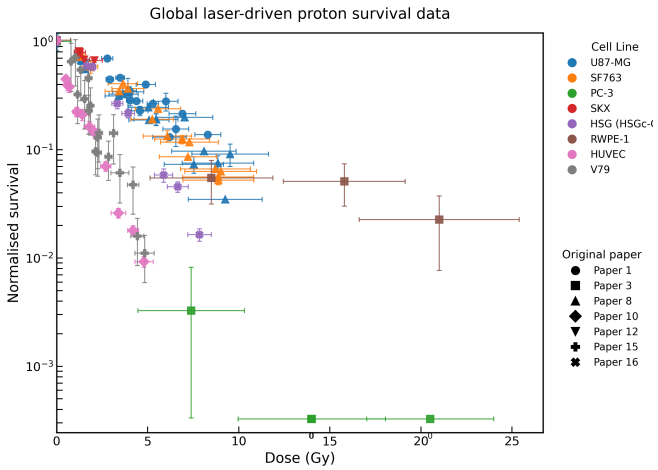


Figure 14: Digitised laser-driven proton survival curve. Marker shape identifies the publication ID (see table 2). Colour identifies the cell line used. Zero-survival observations are displayed at the bottom of the plot, indicated by a 0 below.

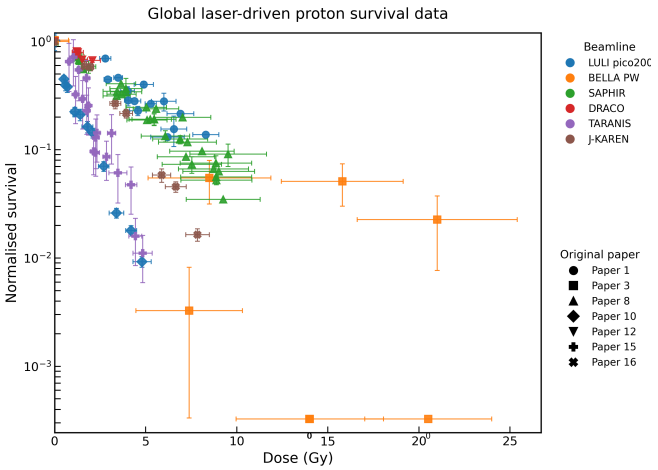


Figure 15: Digitised laser-driven proton survival curve. Marker shape identifies the publication ID (see table 2). Colour identifies the facility/beamline used. Zero-survival observations are displayed at the bottom of the plot, indicated by a 0 below.

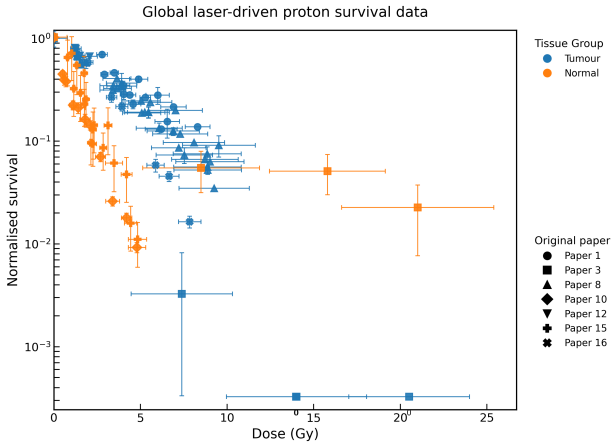


Figure 16: Digitised laser-driven proton survival curve. Marker shape identifies the publication ID (see table 2). Colour identifies the nature (tumour/normal) or the cell line used. Zero-survival observations are displayed at the bottom of the plot, indicated by a 0 below.

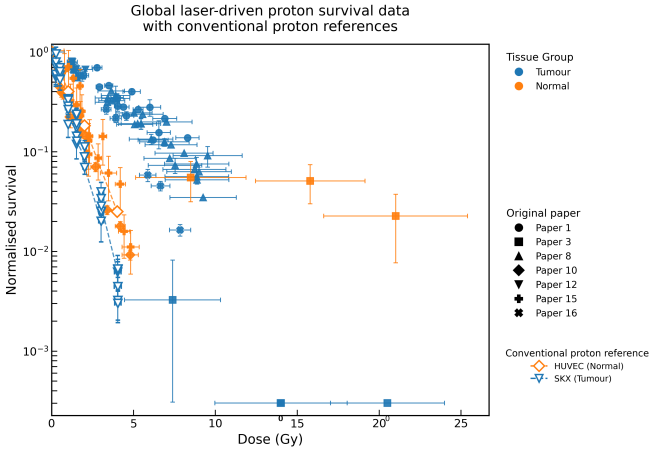


Figure 17: Global laser-driven survival points with digitised conventional-proton reference curves from HUVEC (Paper 10) and SKX (Paper 12). Open dashed series are reference protons; filled points are laser-driven datasets.

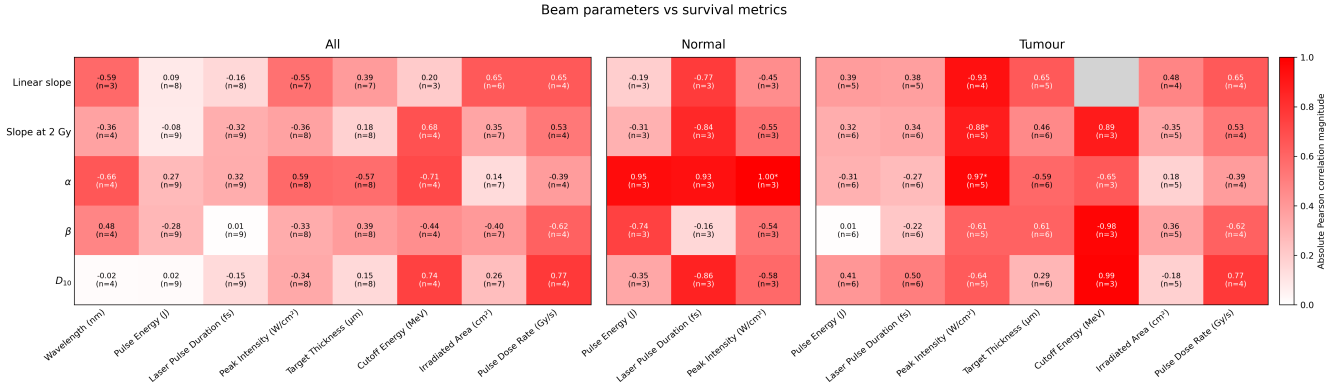


Figure 18: Global Pearson correlations between beam parameters and survival-curve fit metrics. The graphs are split into 3; all cells (left), normal cells only (middle) and tumour cells only (right). Colour shows $|r|$ and text shows signed r with n. Asterisks indicate $p < 0.05$. Removed or grey cells/rows are a result of lack of data (n≤2).

6.2 Early γH2AX foci detection

The extracted early γH2AX foci data show variable dose-dependent increases in γH2AX-containing foci across the different cell lines, displayed in figure 22. All of these cell lines are tumour cells. The variability is likely due to variation in cell radiosensitivity though time point may have an effect. Figure 23 colours the markers in 2 categories; 30 minutes post irradiation

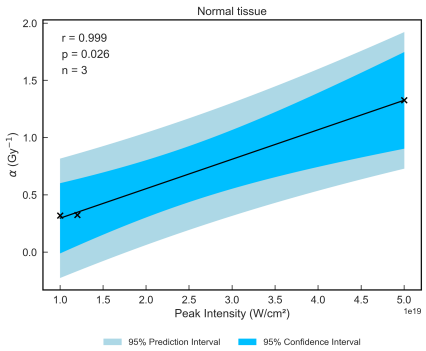


Figure 19: Plot of Peak Intensity vs α (normal cells only).

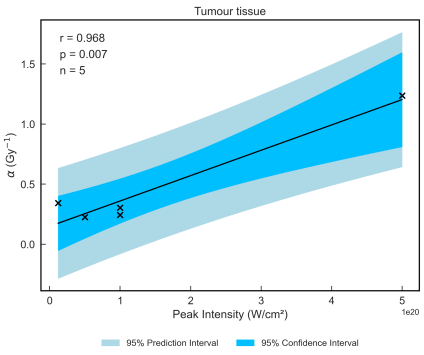


Figure 20: Plot of Peak Intensity vs α (tumour cells only).

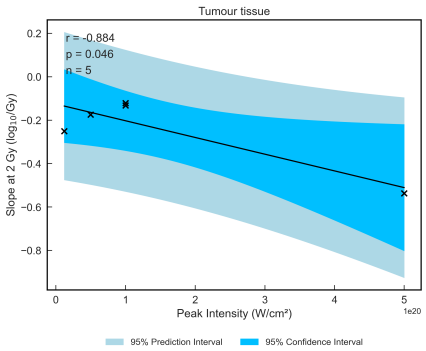


Figure 21: Plot of Peak Intensity vs slope at 2 Gy (tumour cells only).

and 1 hour post irradiation. There appears to be a difference between 30 minutes and 1 hour, however the error bars on the foci counts above 60 from this dataset appear to account for this different. The different cell types and time points make it hard to distinguish any trends in the global data, though it seems like the very general trend agrees with the conventionally accelerated proton, at least for the same cell line.

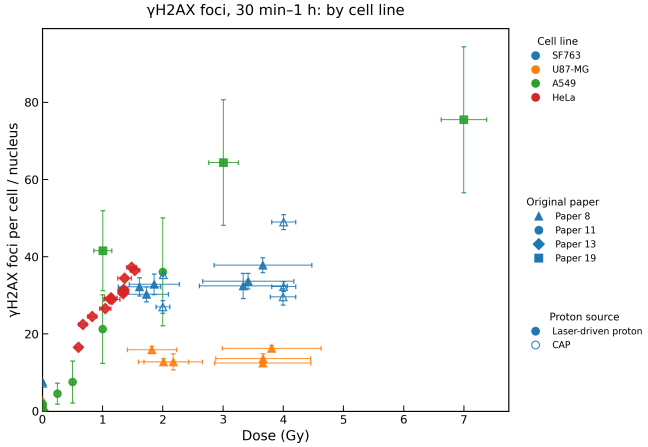


Figure 22: Digitised laser-driven proton γH2AX-containing foci evaluated between 0.5–1 hour post proton irradiation. Marker shape identifies the publication ID (see table 2). Colour identifies cell line. The Paper 8 CAP series is retained as a conventional accelerated proton comparator.

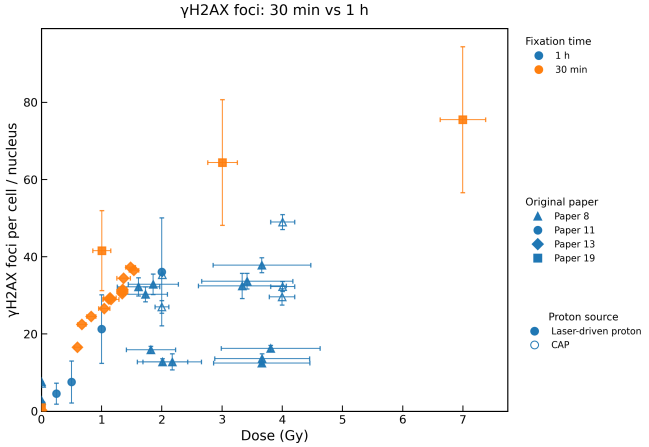


Figure 23: Digitised laser-driven proton γH2AX-containing foci evaluated between 0.5–1 hour post proton irradiation. Marker shape identifies the publication ID (see table 2). Colour identifies evaluation time. The Paper 8 CAP series is retained as a conventional accelerated proton comparator.

6.3 Beam capacity requirements for radiobiology

Table 3 summarises the range of reported irradiation conditions for each radiobiological experiment type (*in vitro* cells, *in vivo* zebrafish embryo and *in vivo* mouse ear). This table indicates the parameter space that has already been demonstrated for laser-driven radiobiology. They also provide a reference point for considering LhARA's Proof-of-Principle LhARA Radiobiology experiment (PoPLaR) at the Scottish Centre for the Application of Plasma-based Accelerators (SCAPA), particularly in terms of whether its present energy, dose, field uniformity and reproducibility fall within the range of existing experiments, and where further development is still required.

Table 3: Beam parameter ranges from the literature for each biological sample irradiated successfully using laser-driven beams.

Sample type	**Area (cm^2)**	**Dose (Gy)**	**Dose per shot (Gy)**	**Max spatial variation (%)**	**Shot-to-shot dose variation (%)**
Cell	0.031–0.785	0.433–37.1 ($n = 33$)	0.0022–3.35 ($n = 31$)	9 ($n = 10$)	9.37–40 ($n = 28$)
Zebrafish embryo	0.00049–0.196	10.37 ($n = 1$)	10.37 ($n = 1$)	10 ($n = 1$)	13.69 ($n = 1$)
Mouse ear	0.196	4 ($n = 1$)	0.66 ($n = 1$)	5 ($n = 1$)	10 ($n = 1$)

7 Evaluation of the PoPLaR beamline for radiobiology

The Proof-of-Principle LhARA Radiobiology experiment (PoPLaR) was constructed to demonstrate the beam transport and radiobiological capability of the laser-driven source at SCAPA. The experiment combined the SCAPA laser-driven proton source with permanent-magnet transport, transverse beam shaping, radiochromic-film (RCF) dosimetry and a dedicated cell carousel for irradiation of FaDu and HeLa cells.

7.1 PoPLaR at the source

The SCAPA laser-driven source is a femtosecond system in the same class as Gemini, DRACO, ATLAS and ELIMAIA, and uses a micrometre-thick Kapton tape rather than the nanometre foils used for the highest-energy femtosecond results. By pulse energy, PoPLaR's proton energy is typical of its class: it aligns with Paper 9 (Gemini, 6 J, 11.1 MeV) and below the DRACO and ELIMAIA results obtained with 8–14 J. Among femtosecond publications, PoPLaR's estimated intensity is about four times the highest intensity in that set (Paper 4 reports a higher value but no proton energy), even though the proton energy doesn't reflect this. For the PoPLaR remit this is less relevant, the beamline being designed for a 10–15 MeV range. For LhARA, the Stage 1 specification calls for higher energies.

Table 4 lists the laser and source parameters of the included publications alongside the parameter values of PoPLaR.

Table 4: Laser and source parameters reported in the included publications (first condition of each paper; blank where not reported) and for PoPLaR. "Max. E_p" is the larger of the reported source cutoff and maximum energy at the sample. Paper 11 reports none of these quantities.

ID	Facility	Energy (J)	Duration (fs)	Intensity (W cm^{-2})	Target	Max. E_p (MeV)
1	LULI PICO2000	100	1200		Au, 12.5 μm	19.6
2	Gemini	12	40	6×10^{20}	C, 15 nm	10 (C ions)
3	BELLA PW	35	45	1.2×10^{19}	Kapton, 13 μm	2.4
4	DRACO	14	30	4.2×10^{21}	plastic, 220 nm	
5	CLAPA	1	30	5.6×10^{19}	plastic, 100 nm	6
6	DRACO	13	30		plastic	19
7	ATLAS-300	2	25		Au, 250 nm	8
8	SAPHIR	3	26	1×10^{20}	Ti, 5 μm	
9	Gemini	6	45	6×10^{20}	a-C, 25 nm	11.1
10	LULI PICO2000	100	1300	5×10^{19}	Au	14
12	DRACO	1.8	30	5×10^{20}	Ti, 2 μm	
13	ATLAS	0.4	30	8×10^{19}	DLC	5.2
14	TARANIS		700	1×10^{19}	Al, 10 μm	5
15	TARANIS	5	500	1×10^{19}	Al, 12 μm	5.3
16	J-KAREN	1	45	5×10^{19}	polyimide, 7.5 μm	4
17	DRACO	3	30		Ti, 2 μm	
18	J-KAREN	0.6	35	5×10^{19}		2.5
19	J-KAREN	1.8	40	7×10^{19}	polyimide, 12.5 μm	4.3
20	VULCAN PW			5×10^{20}	Al, 25 μm	30
21	DRACO					
22	ELIMAIA (L3 HAPLS)	8	30		Al/Cu	40
PoPLaR	**SCAPA**	**5.7–7**	**$\sim$25**	**$\approx$2–2.5$\times 10^{21}$**	**Kapton, 12.7 μm**	**11.8 (median); 16.4 (max)**

The SCAPA source was characterised using Thomson-parabola measurements to reconstruct the proton spectra displayed in figure 24. The corresponding fitted cutoff-energy distribution is shown in figure 25, exhibiting proton cutoff energies extending approximately from 12 to 16 MeV, centred near 14 MeV. These energies place PoPLaR comfortably within the regime already demonstrated for laser-driven *in vitro* radiobiology as the literature review shows that cell irradiation has been demonstrated using proton beams spanning only a few MeV up to tens of MeV.

7.2 PoPLaR at the cells

After the source, a transport section of the beam was added to deliver the beam to the cell carousel. This consisted of two permanent-magnet quadrupoles (PMQs), each with a 10-mm aperture and a magnetic-field gradient of approximately 150 T m^{-1}, designed and positioned using Bayesian optimisation, followed by a 10μm copper scattering foil, selected to minimise lateral variation while retaining as many higher energy protons as possible. A geometric schematic of this set up is given in figure 26.

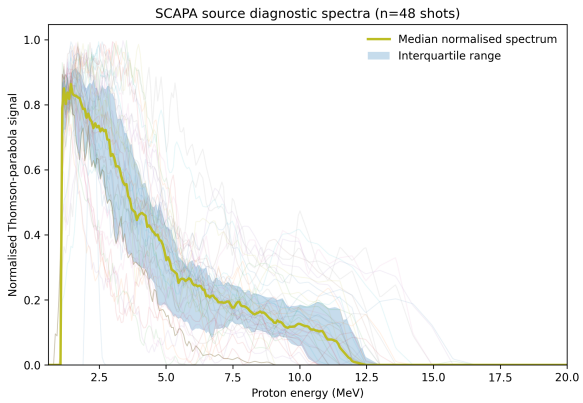


Figure 24: Thomson-parabola source spectra recorded at the SCAPA laser-driven proton source. Individual spectra are normalised to their maximum response; the central curve and shaded region show the median spectral shape and interquartile range.

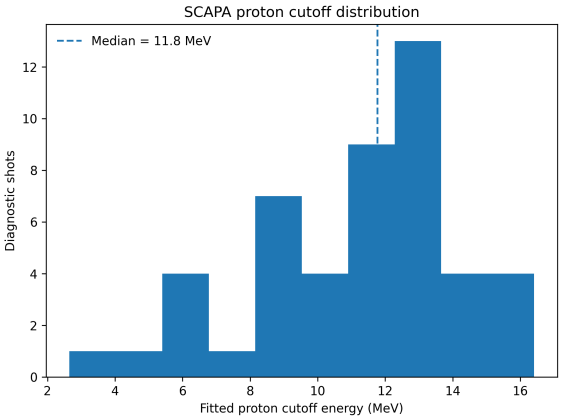


Figure 25: Distribution of fitted proton cutoff energies from the available SCAPA Thomson-parabola source diagnostics.

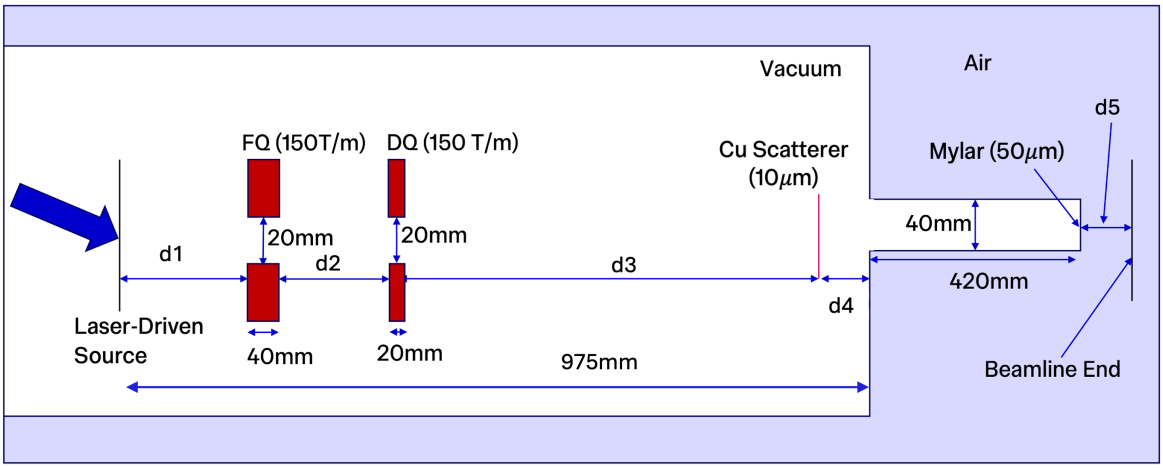


Figure 26: PoPLaR beamline schematic [27].

RCF was used to reconstruct both the absolute dose and transverse distribution at the end of the beamline. Films were mounted in the same carousel geometry used for the biological samples. Small RCF pieces reproduced the cell-carousel geometry, while larger 5×5 cm^2 films were used to characterise the complete cell-dish field. Figure 27 shows the measured dose as a function of shot number.

These doses are in the suitable range for clonogenic cell-survival experiments. The important limitation is instead that the dose could only be established retrospectively. A shot-resolved diagnostic is therefore more immediately important to PoPLaR than simply increasing the available dose. This dose range also overlaps with the dose range required for zebrafish irradiation and mouse ear (see table 3), but increasing the available dose would be necessary for *in vivo* animal models with deeper than surface level irradiation.

Spatial uniformity was quantified using the coefficient of variation of dose across the cell-dish region. The PoPLaR configuration produced a mean CV of 13.93. Figure 28 shows that CV exhibited no obvious dependence on total delivered dose, suggesting that the field structure is primarily determined by beam transport and scattering rather than simply by the number of accumulated shots.

Importantly, this limitation was shown experimentally to be adjustable. Moving the 10 μm Cu scatterer from 669 mm to 305 mm downstream of the second PMQ reduced the mean CV from 13.93% to 8.38%. The improved uniformity was accompanied by a reduction in mean dose per shot from 0.57 to 0.27 Gy, so shot numbers will need to be increased in parallel. The measured change is shown in figure 29.

This result is particularly important because it demonstrates that the spatial non-uniformity is not a fundamental source limitation. An approximately 8% CV already places the improved PoPLaR configuration within the broad range achieved by several published laser-driven radiobiology systems.

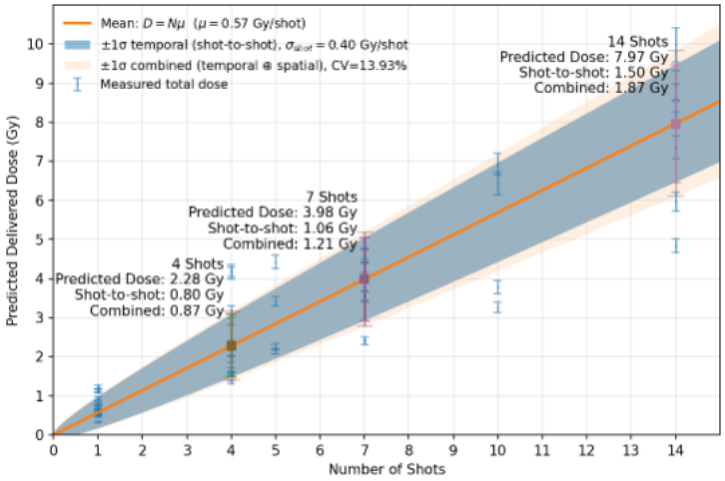


Figure 27: Reconstructed dose as a function of the number of laser-driven proton shots, showing the influence of shot-to-shot variability on the accumulated dose.

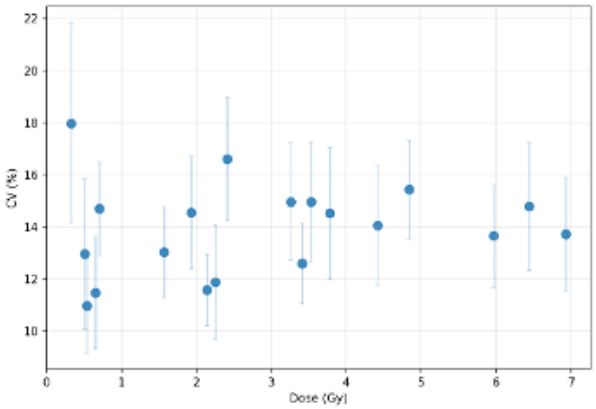


Figure 28: Coefficient of variation of the spatial dose distribution as a function of delivered dose for the large-film measurements [27].

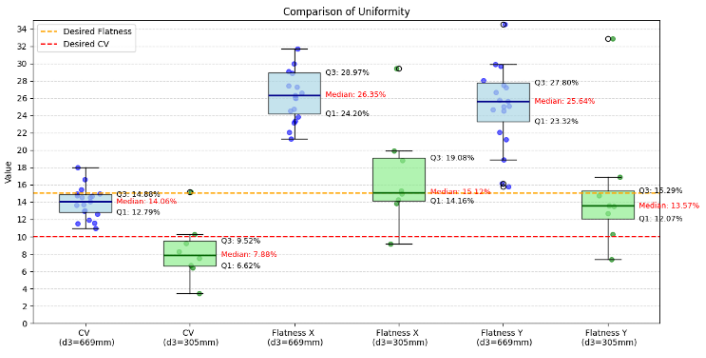


Figure 29: Effect of moving the 10 μm Cu scatterer from 669 mm to 305 mm downstream of PMQ2. The closer scatterer substantially improves transverse uniformity at the cost of reduced dose per shot [27]

.

7.3 PoPLaR radiobiology: Clonogenic survival

During the PoPLaR experiment, the first *in vitro* irradiations of biological samples using SCAPA laser-driven protons were carried out. A mean dose of 0.57 Gy per shot was delivered, with the beam uniformity coefficient of variation of 13.9%. FaDu and HeLa cells were used, though due to incubation issues and the cells being vertical for too long, only some of the FaDu irradiated cells were suitable for data record.

Cell seeding

Hypopharyngeal squamous cell carcinoma cells (FaDu) were purchased from ATCC (Teddington, UK) and authenticated by STR profiling. Cells were cultured as monolayers at 37 °C in 5% CO_2 in Modified Eagle Medium (MEM) supplemented with 10% foetal bovine serum, 2 mM L-glutamine, 1× penicillin–streptomycin and 1× non-essential amino acids. Cells were seeded into in custom dishes made from a glass ring with a thin Mylar film sealed across the bottom and left overnight to attach to the Mylar after seeding before the irradiations. The ring has an inner radius of 18.5 mm, giving a growth area of $\pi\,(1.85\ \mathrm{cm})^2 \approx 2.7\ \mathrm{cm}^2$, comparable to a standard 35 mm dish. Cells grow directly on the Mylar so protons enter through the thin film into the cell monolayer with little energy loss before the cells.

Irradiation

During irradiation, dishes were mounted in a carousel that holds them vertically in the beam path so that several samples can be irradiated in sequence. This resulted in the top half portion of the cells in each dish being uncovered by media during the irradiations. Irradiations occurred in batches of 6; 3 × cell dish irradiations and 3 × RCF irradiations. Unfortunately, it was not possible to record the dose given to each cell dish directly with the current setup; accompanying RCF measurements were taken after the cell irradiations but in the same batch.

Dose was set by the number of laser shots, as summarised in table 5. From approximating the dose to be roughly 0.57 Gy per shot estimated from RCF shots the day before, the doses were decided to be 1, 2 and 4 Gy. These were obtained by the number of shots described in table 5. The values in table 5 were calculated from the radiochromic film (RCF) calibration.

Table 5: Number of laser shots and delivered dose. Dose values are the mean and 1σ range from RCF approximations.

Plan label	Shots	Mean dose (Gy)	1σ range (Gy)	$\pm1\sigma$ (Gy)	Relative (%)
1 Gy	4	2.28	1.42–3.14	0.86	38
2 Gy	7	3.99	2.79–5.19	1.20	30
4 Gy	14	7.97	6.07–9.87	1.90	24

Clonogenic assay

Post-irradiation, cells were washed, trypsinised and seeded into 6 well plates to be left for 1 week to grow and form colonies. Unirradiated control dishes were prepared in the same way and handled alongside the irradiated dishes. Several seeding densities were allocated per dose so that at least one density would give a countable number of colonies whatever the survival turned out to be. Higher doses were given higher densities to accommodate the expected cell death (table 6).

Table 6: Seeding densities (cells per 2.7 cm^2 dish). Day 3 used 500, 1000, 2000 and 4000 cells per dish for every repeat.

Dose (plan label)	Seeding density (cells/dish)		
0 Gy (control)	125	250	500
1 Gy (4 shots)	250	500	1000
2 Gy (7 shots)	500	1000	2000
4 Gy (14 shots)	1000	2000	4000

After 7 days, colonies were fixed and stained with 6% glutaraldehyde and 0.5% crystal violet for 30 min, washed to remove excess stain and left to air-dry overnight. Colonies were counted with a GelCount colony analyser (Oxford Optronics, Oxford, UK), using settings optimised for FaDu (inclusion of distinct colonies of a specific size and intensity) and kept the same for every dish.

Data analysis

The surviving fraction (SF) of each irradiated dish is calculated using the formula given in equation 8.

$$\mathrm{SF} = \frac{\text{colonies counted}}{\text{cells seeded} \times \mathrm{PE}}. \tag{8}$$

For the dose-response curve, the SF values from days 1 and 2 at the same number of shots were combined. The vertical error bars are the standard deviation of the individual dish SF values at that dose. For day 3, the SF of each repeat is the mean over its seeding densities. The reported value is the mean of the three repeats, with the standard deviation of the three repeats as its uncertainty.

The surviving fractions are presented in table 7 and compared with published laser-driven and conventional proton irradiation data in figure 30. The preliminary results are of a similar order of magnitude to previously reported laser-driven proton survival data. Despite the use of tumour cells in this experiment, the surviving fractions at 2.28 Gy and 3.99 Gy appear to align more closely with the published normal tissue trend, while the result at 7.97 Gy shows greater agreement with the tumour tissue trend.

As these results were obtained during a preliminary proof-of-principle experiment, the available data are limited, with three experimental repeats not achieved at all dose points and the reported doses being approximate. As the beamline, experimental

setup and procedures are further developed, improvements in dosimetry and experimental reproducibility are expected to enable more accurate dose measurements and consistent repeats, allowing for more reliable comparisons with published survival data.

Table 7: FaDu dose-response surviving fractions (days 1–2 combined). n is the number of dishes contributing. Dashes in the raw data, i.e. dishes without a usable count, are not included in n.

Shots	Dose (Gy)	SF	n (dishes)
4	2.28 ± 0.86	0.178 ± 0.072	8
7	3.99 ± 1.20	0.097 ± 0.019	6
14	7.97 ± 1.90	0.127	1

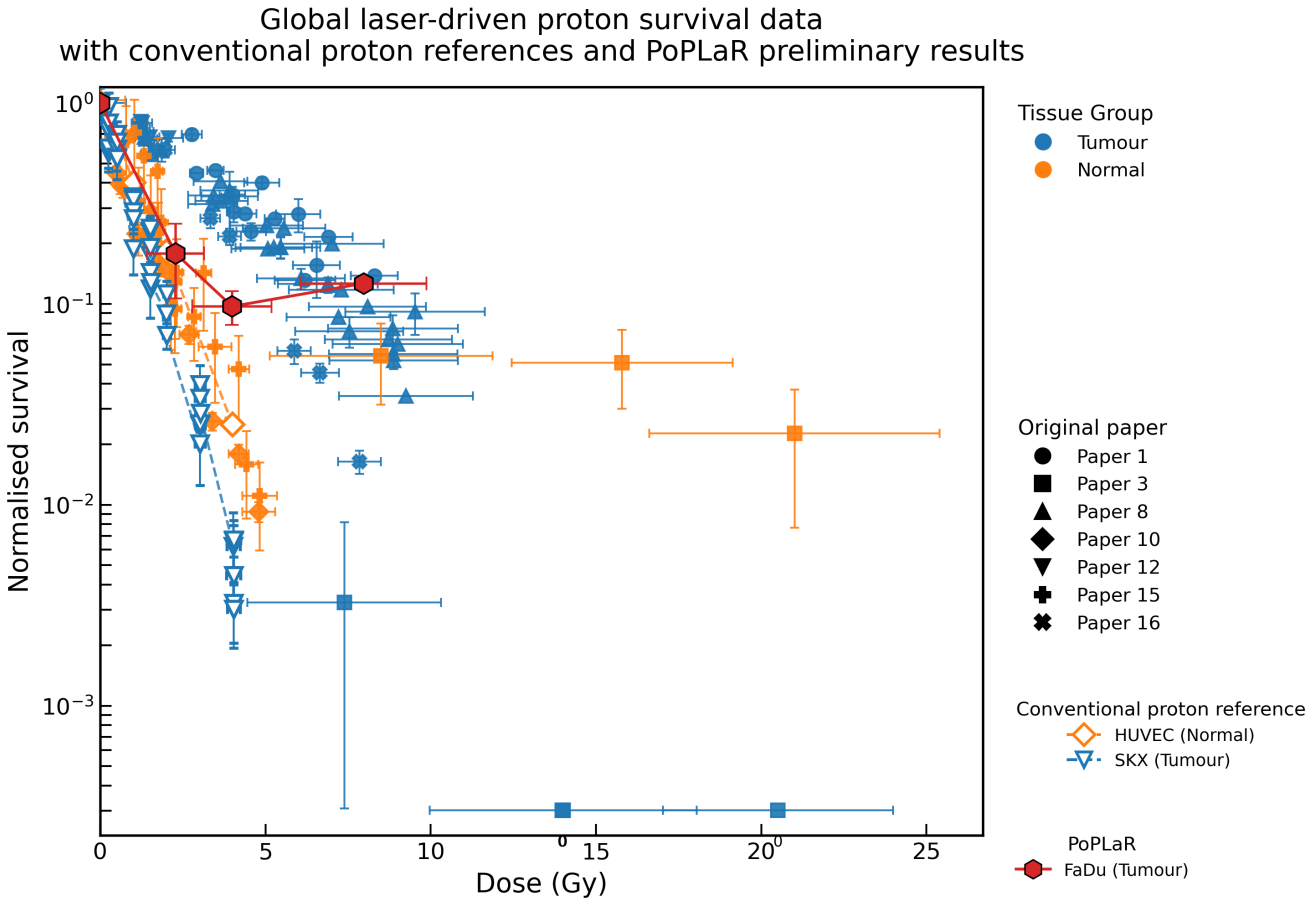


Figure 30: PoPLaR FaDu preliminary survival results (red hexagons) added to the previous global laser-driven proton survival plot (17). Horizontal error bars are the RCF 1σ dose range; vertical error bars are the standard deviation across dishes (none is shown at 14 shots, where only one dish was usable).

Shot-to-shot reproducibility

A second experiment was also conducted to test how reproducible survival is from one 4-shot irradiation to the next, and see how shot-to-shot variation may impact survival. Estimating a dose of 0.57 Gy per shot, this should equate to a dose of 2.28 ± 0.86 Gy delivered to each cell dish.

The three independent 4-shot irradiations resulted in surviving fractions of 0.111, 0.116 and 0.138 (table 8), corresponding to a coefficient of variation of approximately 12%. This indicates that, at this dose level, shot-to-shot fluctuations in the laser-driven source did not produce large differences in clonogenic survival. However, this conclusion is limited by the dosimetry: as dose was recorded only on RCF irradiated after the cell dishes. The dose delivered to each dish therefore remains uncertain, and therefore the agreement between repeats might simply reflect low shot-to-shot variation during these three irradiations specifically.

Table 8: Shot-to-shot reproducibility experiment results: three independent 4-shot (2.28 ± 0.86 Gy) irradiations. SF for each repeat is the mean over its seeding densities; n is the number of dishes with a usable count.

Repeat	SF	n (dishes)
1	0.111	4
2	0.116	2
3	0.138	4
Mean $\pm$ SD	0.122 ± 0.014	3 repeats

PoPLaR limitations & proposed mitigations

As noted, there were limitations within the PoPLaR experiment. These initial technical challenges will inform the next phase of the PoPLaR experiment; these are:

- **Time held vertically in the carousel:** In the carousel the dishes are held vertically, so the cells are suspended for the duration of cell irradiations and subsequent RCF irradiations, with reduced medium coverage and outside the incubator. Irradiating RCF in the same carousel alongside the cells meant extra positions to cycle through, which lengthened the time every dish spent vertical.
- **Dose uncertainty:** Dose was measured only on RCF next to the dishes, not on each dish for each shot, so the dose assigned to every dish is an average over shots. Combined with the shot-to-shot variation of the laser-driven source, this gives 1σ dose uncertainties of 24–38 (table 5). With uncertainties this large, the doses at 4 and 7 shots overlap within 1σ, and the data cannot constrain the shape of the survival curve.
- **Incubator malfunction:** An incubator malfunction during the beamtime affected all of the HeLa dishes and some the FaDu dishes during the 7 day growth period, meaning that repeats were lost and a second cell line validation was not possible during this experimental phase.

Future PoPLaR phases will measure dose on a per-dish basis in real time. Cells will grow on a transwell membrane with a piece of RCF directly beneath it, so every dish has its own film record of the dose actually delivered. A scintillating fibre around the outside of each dish will provide a dose signal on every shot. Monte Carlo simulations will then relate the scintillator signal to the dose at the cell layer. This will give a real-time estimate of the dish dose while the experiment is running. Knowing the delivered dose immediately means the seeding density choice can be informed better for clonogenic assays. This method of plating and dose calculation means that the cells will not need to be suspended longer to irradiate acompanying RCF and the transwell plates should keep the cells moist during irradiation regardless of media coverage.

7.4 PoPLaR radiobiology: current assessment and development priorities

Table 9 is an extension of table 3, including PoPLaR's parameters recorded during the clonogenic survival proof-of-principle experiment for comparison. PoPLaR appears to demonstrate most of the fundamental components required for a laser-driven *in vitro* radiobiology platform; the capture and transport of a highly divergent laser-driven proton source, a biologically useful dose per shot and cumulative doses spanning the conventional clonogenic range, resulting in the first irradiation of cells at this beamline.

PoPLaR's proton energy, dose-per-shot and achievable total dose already lie within the global ranges established by laser-driven proton radiobiology experiments (table 9), while its demonstrated spatial uniformity is approaching that of established systems. The main current limitation is reproducibility, shot-to-shot variability and real-time knowledge of the beam delivered to each biological sample. Addressing this limitation would move PoPLaR from a commissioning experiment towards a quantitatively controlled radiobiology platform suitable for repeated biological studies and, subsequently, for direct integration into the wider LhARA programme.

8 Evaluation of PoPLaR for new modalities of radiotherapy

FLASH (ultra-high dose-rate) radiotherapy and minibeam radiation therapy (MBRT) modify delivery in the temporal and spatial domains respectively. FLASH is defined by dose rate beams exceeding 40 Gy/s; MBRT uses beam segments of 1 mm or less, typically 500–700 μm, separated by a few millimetres [28]. Both have been evidenced to exhibit normal-tissue sparing with maintained tumour control in pre-clinical studies but require a wider range of research to bridge the gap from pre-clinical to clinical, an aim of the LhARA collaboration.

Table 9: Existing laser-driven *in vitro* experimental characteristics in comparison to PoPLaR.

Sample type	**Area (cm^2)**	**Dose (Gy)**	**Dose per shot (Gy)**	**Max spatial variation (%)**	**Shot-to-shot dose variation (%)**
Cell	0.031–0.785	0.433–37.1 ($n = 33$)	0.0022–3.35 ($n = 31$)	9 ($n = 10$)	9.37–40 ($n = 28$)
Zebrafish embryo	0.00049–0.196	10.37 ($n = 1$)	10.37 ($n = 1$)	10 ($n = 1$)	13.69 ($n = 1$)
Mouse ear	0.196	4 ($n = 1$)	0.66 ($n = 1$)	5 ($n = 1$)	10 ($n = 1$)
PoPLaR	∼2.7	∼2.28–7.97	∼0.57	∼13.93	∼23.84–37.72

8.1 FLASH

Table 10 presents an overview of the global energy and dose ranges used in different proton FLASH radiobiological experiments. The ranges were compiled from the proton studies identified in a FLASH review and thesis, supplemented by the corresponding primary literature [29, 30] whereby a database was created to investigate the current literature surrounding FLASH radiobiology.

Table 10: Beam parameter ranges from the literature for each biological sample irradiated successfully using FLASH proton beams.

Environment	Biological model	Particle energy (MeV)	Total dose (Gy)	Mean dose rate (Gy/s)
In vitro	Cells	4.5–20	0.5–20	10–1000
In vivo	Zebrafish	68–228	9–43	100–9000
In vivo	Mouse	20–250	10–60	57–930
In vivo	Rat	226–250	5–25	60–257

PoPLaR's source energy lies within the range used for proton FLASH studies on cultured cells, and its cumulative doses of ∼2.28–7.97 Gy overlap the lower part of the *in vitro* and rat ranges. The instantaneous dose rate within each bunch is intrinsically very high, but the mean dose rate over a multi-shot exposure is below the conventional 40 Gy/s criterion: the repetition rate was not recorded, but at SCAPA's maximum of 5 Hz, 0.57 Gy per shot corresponds to less than 3 Gy/s.

A FLASH-relevant exposure with PoPLaR would therefore need to be a single shot or a few shots, which requires an on-shot dose measurement. PoPLaR can contribute to the question of whether instantaneous or mean dose rate governs the response, provided both are reported. It cannot currently reproduce conventional *in vivo* FLASH conditions with its current setup, which need higher energy and dose per exposure.

8.2 MBRT

Table 11 presents an overview of the global energy and dose ranges used in different proton FLASH radiobiological experiments. The ranges were compiled from the proton studies identified in a FLASH review and thesis, supplemented by the corresponding primary literature [29, 30] whereby a database was created to investigate the current literature surrounding FLASH radiobiology.

Similar to table 10, table 11 presents an overview of the global energy and dose ranges used in different radiobiological experiments, but for minibeams. The ranges were also compiled from the proton studies identified in a SFRT review and the same thesis, supplemented by the corresponding primary literature [29, 31].

Table 11: Beam parameter ranges from the literature for each biological sample irradiated successfully using MBRT proton beams.

Environment	Biological model	Particle energy (MeV)	Total dose (Gy)
In vitro	Cells	100	2–20
In vivo	Mouse	20–100	20–30
In vivo	Rat	100	10–30

The present PoPLaR dose range overlaps with the lower end of the *in vitro* MBRT irradiation range, however, the lateral variability in the beam may be a limitation, as the literature suggests that the biological result relies on peak and valley doses in MBRT [31]. With a CV of 13.93%, dose across the irradiated cellular areas may the doses in the peaks and valleys. As

displayed in figure 29, moving the 10 μm Cu scatterer from 669 mm to 305 mm downstream of PMQ2 should reduce this variation to 8.38%.

The current PoPLaR experiments are not yet compatible with *in vivo* experimentation, being below the dose range and energy range for both rodent species used in the current literature. As PoPLaR advances, embryo and rodent species would be a part of the irradiation programme, once energy, dose and variability improve.

For FLASH, the LhARA collaboration aims to provide unique temporal structures and for MBRT, LhARA aims to improve the collimation technique, using magnetic focussing rather than mechanical beam degrading, allowing for peak and valley dose flexibility.

9 Conclusion

The PRISMA-guided review of 22 publications demonstrates that laser-driven proton and ion sources have progressed in their capabilities, with an overall increase in maximum particle energy by publication year. The field remains concentrated at a small number of facilities, with the DRACO beamline at Helmholtz-Zentrum Dresden-Rossendorf accounting for almost 1/4 of all publications. These facilities have demonstrated the ability to perform *in vitro* and low-dose *in vivo* radiobiology experiments, although the literature remains sparse and heterogeneous, particularly for heavy-ion irradiation and *in vivo* studies. Regardless, sustained progress in the field is representable by an observed increase in maximum particle energy at the sample with publication year ($r = 0.921$, $p = 4.97 \times 10^{-10}$), indicating continued improvement/development of laser-driven ion sources.

The irradiation conditions reported across publications are inconsistent, limiting direct comparisons between experiments. Future studies should routinely report particle energy and energy spread at the biological sample, LET where available, dose per pulse, bunch duration at the sample, number of pulses, pulse separation, instantaneous dose rate, mean dose rate, total irradiation time, variation metrics (e.g. shot-to-shot and lateral variation) and associated uncertainties.

Analysis of the global laser-driven irradiated biological data had limited results due to the inconsistency of beam parameters, though survival curve data displays an observable difference in response between normal and tumour tissue under laser-driven proton irradiation. Normal tissue cell lines exhibit steeper survival curves than tumour cell lines in the laser-driven dataset, while reference conventional proton data show survival curves for both tissue types seem to result in a steepness comparable to that of the laser-driven normal tissue curves. The limited size and heterogeneity of the current dataset, with normal tissue represented by only three cell lines from three different facilities, means this observation should be treated as preliminary, but it provides clear motivation for the matched, controlled comparisons that the field currently lacks. The available γH2AX foci data, though sparse, are broadly consistent with conventionally accelerated proton results, with no specific trend. Differences can be observed between time points, though this could be a result of cell line radiosensitivity differences.

PoPLaR represents a clear and significant success: laser-driven protons produced at SCAPA have been successfully transported through a 150 T m^{-1} permanent-magnet quadrupole doublet and copper scatterer, and used to irradiate cells for the first time at this facility. This milestone establishes SCAPA as a viable platform for laser-driven radiobiology and places PoPLaR within the global landscape of such experiments. The beamline delivered 0.57 ± 0.03 Gy per shot to a 2.7 cm^2 area field, with a median proton cutoff energy of 11.8 MeV across 48 characterisation shots. Preliminary FaDu clonogenic survival data at cumulative doses of 2.28, 3.99 and 7.97 Gy are consistent with the global laser-driven dataset order, confirming the biological validity of the irradiation. The spatial coefficient of variation of 13.9% is competitive with established systems and improved to approximately 8% following scatterer repositioning, demonstrating that field uniformity is approaching the standard required for systematic radiobiology. However, dose reproducibility remains a significant limitation, with fluctuations of 23–38% across multi-shot exposures. The absence of an on-shot dose diagnostic further limits the ability to monitor and control individual irradiations. Improving shot-to-shot dose stability, implementing on-shot dosimetry and further optimising field uniformity should therefore be priorities for the next phase of PoPLaR experiments.

With respect to the emerging modalities of FLASH and minibeam radiotherapy, the instantaneous dose rates of laser-driven sources exceed the 40 Gy/s threshold associated with the FLASH effect, and single-shot or few-shot exposures fall within the *in vitro* FLASH dose range. However, the multi-shot cumulative exposures required for most *in vitro* survival studies, delivered at low repetition rates, result in mean dose rates well below the FLASH threshold, meaning the majority of existing laser-driven radiobiology experiments cannot be classified as FLASH irradiations.

Continued improvements in laser-driven source energy, beam transport and dose control will be necessary to extend the range of biological experiments that can be performed. In particular, higher particle energies and improved delivery capabilities would support irradiation of more complex *in vivo* models and further investigation of heavier ion species, for which the current published evidence is extremely limited, with only one carbon-ion study identified in this review. These developments would also support future investigations of FLASH and minibeam radiation therapy (MBRT) under *in vivo* conditions.

References

[1] D. Doria *et al.*, "Biological effectiveness on live cells of laser driven protons at dose rates exceeding 10^9 Gy/s," *AIP Advances* **2** (2012) 011209.

[2] F. Hanton *et al.*, "DNA DSB Repair Dynamics following Irradiation with Laser-Driven Protons at Ultra-High Dose Rates," *Scientific Reports* **9** (2019) 4471.

[3] J. Bin *et al.*, "A new platform for ultra-high dose rate radiobiological research using the BELLA PW laser proton beamline," *Scientific Reports* **12** (2022) 1484.

[4] A. Flacco *et al.*, "Laser driven FLASH radiobiology using a high dose and ultra high dose rate single pulse proton source," *Scientific Reports* **15** (2025) 16511.

[5] F. Kroll *et al.*, "Tumour irradiation in mice with a laser-accelerated proton beam," *Nature Physics* **18** (2022) 316–322.

[6] J. Han *et al.*, "Ultra-High Dose Rate FLASH Irradiation Induced Radio-Resistance of Normal Fibroblast Cells Can Be Enhanced by Hypoxia and Mitochondrial Dysfunction Resulting From Loss of Cytochrome C," *Frontiers in Cell and Developmental Biology* **9** (2021) 672929.

[7] F.-E. Brack *et al.*, "Spectral and spatial shaping of laser-driven proton beams using a pulsed high-field magnet beamline," *Scientific Reports* **10** (2020) 9118.

[8] T. F. Rösch *et al.*, "A feasibility study of zebrafish embryo irradiation with laser-accelerated protons," *Review of Scientific Instruments* **91** (2020) 063303.

[9] E. Bayart *et al.*, "Fast dose fractionation using ultra-short laser accelerated proton pulses can increase cancer cell mortality, which relies on functional PARP1 protein," *Scientific Reports* **9** (2019) 10132.

[10] L. Manti *et al.*, "The radiobiology of laser-driven particle beams: focus on sub-lethal responses of normal human cells," *Journal of Instrumentation* **12** (2017) C03084.

[11] S. Raschke *et al.*, "Ultra-short laser-accelerated proton pulses have similar DNA-damaging effectiveness but produce less immediate nitroxidative stress than conventional proton beams," *Scientific Reports* **6** (2016) 32441.

[12] K. Zeil *et al.*, "Dose-controlled irradiation of cancer cells with laser-accelerated proton pulses," *Applied Physics B* **110** (2013) 437–444.

[13] J. Bin *et al.*, "A laser-driven nanosecond proton source for radiobiological studies," *Applied Physics Letters* **101** (2012) 243701.

[14] F. Fiorini *et al.*, "Dosimetry and spectral analysis of a radiobiological experiment using laser-driven proton beams," *Physics in Medicine & Biology* **56** (2011), no. 21, 6969–6982.

[15] A. Yogo *et al.*, "Measurement of relative biological effectiveness of protons in human cancer cells using a laser-driven quasimonoenergetic proton beamline," *Applied Physics Letters* **98** (2011) 053701.

[16] S. D. Kraft *et al.*, "Dose-dependent biological damage of tumour cells by laser-accelerated proton beams," *New Journal of Physics* **12** (2010) 085003.

[17] A. Yogo *et al.*, "Application of laser-accelerated protons to the demonstration of DNA double-strand breaks in human cancer cells," *Applied Physics Letters* **94** (2009) 181502.

[18] A. Yogo *et al.*, "Measurement of DNA double-strand break yield in human cancer cells by high-current, short-duration bunches of laser-accelerated protons," *Japanese Journal of Applied Physics* **50** (2011), no. 10, 106401.

[19] P. Chaudhary *et al.*, "Development of a portable hypoxia chamber for ultra-high dose rate laser-driven proton radiobiology applications," *Radiation Oncology* **17** (2022) 77.

[20] J. Metzkes-Ng *et al.*, "The dresden platform is a research hub for ultra-high dose rate radiobiology," *Scientific Reports* **13** (2023) 20611.

[21] P. Bláha *et al.*, "ELIMAIA-ELIMED: a new user platform for radiobiological research utilizing laser-driven protons," *Frontiers in Physics* **13** (2025) 1567622.

[22] P. Chaudhary *et al.*, "Cellular irradiations with laser-driven carbon ions at ultra-high dose rates," *Physics in Medicine & Biology* **68** (2023) 025015.

[23] K. Pearson, "Notes on Regression and Inheritance in the Case of Two Parents," *Proceedings of the Royal Society of London* **58** (1895) 240–242.

[24] *Biometrika* **6** (1908), no. 2-3, 302–310.

[25] D. Howell, "Correlation and Regression," *Statistical Methods for Psychology* (2010) 245–283.

[26] S. J. McMahon, "The linear quadratic model: usage, interpretation and challenges," *Phys. Med. Biol.* **64** (Dec., 2018) 01TR01.

[27] C. Dyson, E. Melia, and J. McGarrigle, "PoPLaR – SCAPA Phase 2," tech. rep., LhARA collaboration, 2025. Draft report; TN number to be assigned.

[28] H. Ahmed *et al.*, "ITRF/LhARA conceptual design report," Tech. Rep. STFC-TR-2026-007, STFC Rutherford Appleton Laboratory, 2026.

[29] McGarrigle, Josie May, "Exploring new approaches in radiotherapy to optimise the design of LhARA,".

[30] J. M. McGarrigle, K. R. Long, and Y. Prezado, "The FLASH effect—an evaluation of preclinical studies of ultra-high dose rate radiotherapy," *Frontiers in Oncology* **14** (Apr., 2024).

[31] J. M. McGarrigle, K. R. Long, and Y. Prezado, "On the significance of the different geometrical and dosimetric parameters in microbeam and minibeam radiation therapy a retrospective evaluation," *Frontiers in Oncology* **14** (2024).